Journal of Alloys and Compounds 508 (2010) 184–190

Contents lists available at ScienceDirect

Journal of Alloys and Compounds

journal homepage: www.elsevier.com/locate/jallcom

# Synthesis of $Pb_{1-x}R_xZr_{0.65}Ti_{0.35}O_3$ ($x = 0.05$, 0.10 and 0.15; R = Ce, Pr and Nd) powders by Gel Entrapment Technique and study on their thermo-physical and electrical properties

Rajesh V. Pai [a,*], R. Mishra [b], M.R. Pai [b], S.K. Mukerjee [a], V. Venugopal [c]

[a] Fuel Chemistry Division, Bhabha Atomic Research Centre, Mumbai 400 085, India
[b] Chemistry Division, Bhabha Atomic Research Centre, Mumbai 400 085, India
[c] RC&I Group, Bhabha Atomic Research Centre, Mumbai 400 085, India

ARTICLE INFO

*Article history:*
Received 10 May 2010
Received in revised form 8 August 2010
Accepted 12 August 2010
Available online 19 August 2010

*Keywords:*
Ferroelectrics
X-ray diffraction
Impedance

ABSTRACT

Rare earth doped lead zirconate titanate of composition $(Pb_{1-x}R_xZr_{0.65}Ti_{0.35})O_3$ where $x = 0$, 0.10 and 0.15 and R = Ce, Pr and Nd was prepared by Gel Entrapment Technique (GET). The gel was suitably calcined at 1073 K and the resultant product was characterized by XRD, SEM, BET surface area analysis and Dynamic Light Scattering. The dielectric constants of PZT were found to decrease with Ce doping where as it increased with Pr doping. The pyrochlore phase in Nd doped samples was found to be responsible for lower conductivity and dielectric constant values. The redox behaviour of the compounds was studied by TPR–TPO measurements.



## 1. Introduction

Lead zirconate titanate (PZT) [1] ceramics have been used extensively for various device applications because of their excellent dielectric, pyroelectric, piezoelectric and electro optic properties [2]. PZT is a perovskite $ABO_3$ solid-state solution wherein the B-site composition can be continuously varied from the titanium-free $PbZrO_3$ (PZ) at one extreme to pure $PbTiO_3$ (PT) at the other. The ratio of Zr to Ti dramatically affects the properties of the PZT materials and is often represented numerically in an abbreviation, such as PZT (30/70), where the composite ratio is 30% Zr and 70% Ti. Optimal excess PbO addition and rapid heating to the annealing temperature are found to lead to improved electrical characteristics [3,4]. The inclusion of acceptor or donor dopants (i.e. the charge of the dopant being lower or higher than the metal cation for which it substitutes) is often used to alter the properties of PZT by suppressing or promoting oxygen or cation vacancies [5,6]. While there have been substantial improvements in many of the properties of PZT using acceptor and donor dopants, it is important to garner greater understanding and control over the properties of ferroelectric materials. Although a great deal of research has focused on doping PZT with $La^{3+}$ [5,7] and a number of the other individual lanthanide ($Ln^{3+}$) cations, few systematic Ln doping PZT studies have been reported on ceramics [8–10]. Initially, it was important to discern where the Ln dopants would most likely reside in the $ABO_3$ structure (i.e., A- or B-site dopants). As a starting rationale, the rules of Goldschmidt suggest that dopants will reside on a specific lattice site (either A or B) if a dopant ion's radius is within 15% of the replaced ion [11]. Additionally, it has been shown that the Ln cations will occupy both the A and B sites [5,8–10,12,13–15] but the preference for B-site occupancy increases as the radius of the dopant decreases [8,9,14].The decrease in cation size from 1.17 Å (La) to 1.00 Å (Lu) [16] results in a transition from A-site ($rPb^{2+} = 1.2$ Å) to B-site ($rTi^{4+} = 0.68$ Å, $rZr^{4+} = 0.79$ Å) occupancy. For intermediate ionic radii values, shared site occupancy (also termed amphoteric or self-compensating) has been shown for trivalent dopants in other perovskite systems, such as $BaTiO_3$ [17] and $SrTiO_3$, [13] and has been predicted for PZT (95/5) [8,9]. Therefore, in the PLnZT system, the $Ln^{3+}$ ions may compensate for a pair of missing $Pb^{2+}$ and $B^{4+}$ (Ti or Zr) cations. The studies conducted by Sharma et al. [14] for the $(Pb_{1-3x/2}Ln_x)(Zr_{0.65}Ti_{0.35})O_3$ system indicated a dominant A-site occupancy for the early Ln cations. The Ce dopant in their study was assumed to be +3 (1.03 Å) and thus occupy the A site; however, other studies indicate that the Ce cation is in fact in the +4 (0.92 Å) state, and thus, B-site occupancy in PZT [12] and other perovskite systems [15] would be favored. A mixed A/B site occupancy for Ln dopants in the PZT (95/5) system was predicted by Troccaz et al. using tolerance factor calculations [9].

Conventional method of preparing these ceramic materials is by the solid-state reactions [18,19]. But the advantages of solu-

* Corresponding author. Tel.: +91 22 25504090.
*E-mail address:* pairajesh007@gmail.com (R.V. Pai).

0925-8388/$ – see front matter © 2010 Elsevier B.V. All rights reserved.
doi:10.1016/j.jallcom.2010.08.041

tion based routes lie in the formation of the product at much lower temperatures with larger surface area and better microhomogeneity compared to solid-state route especially for present multicomponent system. Lower synthesis temperatures prevent volatilization of the component oxide facilitating fixing of required stoichiometry. The present paper deals with synthesis of PZT powders containing 5, 10 and 15 mol% Ce, Pr and Nd by Gel Entrapment Technique (GET) [20]. AC impedance spectroscopy has been utilized to study the electrical properties such as dielectric properties and electrical conductivity of the samples at different temperatures. Depending on their dopant ion concentration the electrical properties have been modified/deteriorated due to the different site occupancy. The redox behaviour of these compounds have also been investigated was studied by Temperature Programmed Reduction–Oxidation (TPRO) studies to determine the stability under reducing atmosphere.

## 2. Experimental

The PZT gel precursors containing varying amounts of rare earths were prepared by Gel Entrapment Technique [21]. For this titanium (IV) nitrate solution was prepared by precipitating titanium trichloride into titanium hydroxide by addition of liquor ammonia and then redissolving hydroxide in concentrated nitric acid over an ice-bath. The titanium nitrate solution was stored in the refrigerator. The rare earth (III) nitrate solutions were prepared by dissolving the A.R. grade rare earth oxides in concentrated $HNO_3$. The residual solution was evaporated to dryness. The nitrate crystals of rare earths were then redissolved in 1 M $HNO_3$. Both the nitrate stock solutions along with A.R. grade zirconium oxynitrate were analyzed for their metal contents by gravimetric method. In all compositions, the Zr/Ti molar ratio was constant and maintained at 1.86, while the ratio of Pb/R (R = Nd, Pr and Ce) was 5.667, 9 and 19 when the R was 0.15, 0.10 and 0. 05 respectively. Accordingly appropriate volumes of the metal nitrate solutions were mixed to achieve the required compositions. To this mixture of nitrate solution, 3 M hexamethylenetetramine (HMTA) solution was added gradually at room temperature with constant stirring till a hard gel was obtained. The gel obtained in the process was then dried in an oven at 423 K and heated to 473 K to obtain a fluffy mass of the precursor material. The precursors were further heat treated at 1023 K in air for 4 h to get phase-pure compounds. These precursor powders were further heated to 773 K to remove any leftover organic matter and finally to 1073 K to get phase-pure compounds. The typical flow sheet of powder preparation is given in Fig. 1. The XRD patterns were recorded on an X-ray powder diffractometer using Cu $K_\alpha$ radiation ($\lambda = 1.5406$ Å) with a graphite monochromator to identify the phases. The applied voltage was 45 kV and the current was 30 mA. Characterization of the powder by XRD line-broadening showed a particle size of ~40 nm. Specific surface area of the sample was determined by the BET method. The particle size distribution analysis was carried out by Dynamic Light Scattering (DLS).

Temperature programmed Reduction/Oxidation (TPR/TPO) is a sensitive and specific technique for monitoring the redox property of the species present in the system under reducing oxidizing conditions. TPR run was recorded on a TPDRO-1100 analyzer (Thermo Quest, Italy) under the flow of ($H_2$ (5%) + Ar) and alternatively $O_2$ (5%) + He at a gas flow rate of 20 ml $min^{-1}$, in temperature range 25–1000 °C, at a heating rate of 6° $min^{-1}$.

The powders calcined at 1073 K were cold pressed into pellets of 10 mm diameter and 2 mm thickness using a uniaxial hydraulic press. Sintering of these pellets was carried out at different temperatures from 1173 K to 1373 K. In order to prevent PbO vaporization, an equilibrium PbO vapour pressure was established using $PbZrO_3$ as setter, and placing everything in the covered alumina crucible. The sintered density of the pellets was measured by liquid displacement method.

For the dielectric property measurement, the sintered pellet samples were coated with platinum paste in order to make the pellet conductive. The dielectric constant of these pellets was determined using a Solartron AC Frequency Analyzer (Model 1260) in the frequency range 10 MHz to 1 Hz. The experiments were carried out at different temperatures from 473 K to 873 K in an interval of 25 K. The temperature was controlled by a microprocessor and measured by a K-type thermocouple placed very close to the sample. At each temperature, the samples were equilibrated for 20 min before recording the spectra.

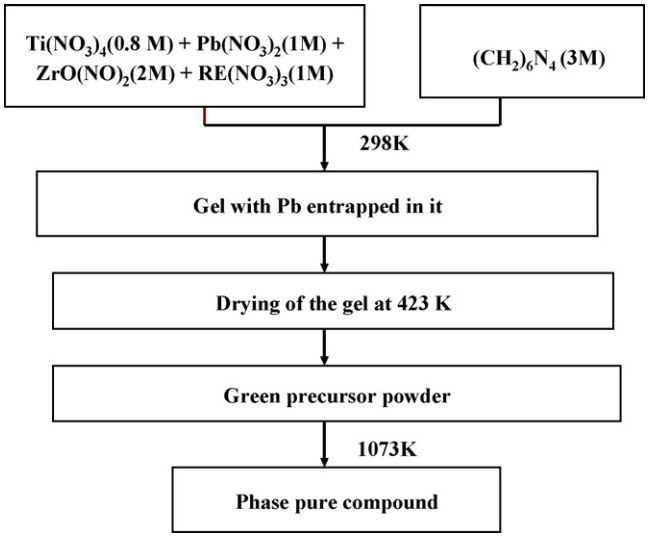


**Fig. 1.** Flowsheet used for the preparation PZT powders.

## 3. Results and discussion

The room temperature XRD analysis of the samples heated to 1073 K indicated that the materials were single phase with cubic lattice structure except for Nd substituted samples in which some pyrochlore phases were also observed. Pyrochlore phase is usually formed as a transient phase [22] before the PZT formation. From Fig. 2, it can be seen that the onset of formation of the pyrochlore phase was evolved in the precursor stage along with some other impurity phases, apart from the cubic phase. Even though these impurity phases disappeared on further heating to 1023 K, the pyrochlore phases remained in the Nd containing samples. The pyrochlore phase in Nd containing samples found to increase with the increase in Nd content. Phase pure cubic phases were obtained for 5, 10 and 15 mol% Ce and Pr doped samples. The cell parameters of the compounds obtained from least square fitting of the XRD data were found to be in good agreement with the reported values. Fig. 3 shows the room temperature XRD patterns of these compounds calcined at 1073 K. The sharp and singlet pattern indicates better phase purity and crystallinity. In this system Pb loss due to uncontrolled heating during self-propagating ignition of dried gel is a matter of concern. However, in the present study it was found that there was no Pb loss as the maximum temperature attained by

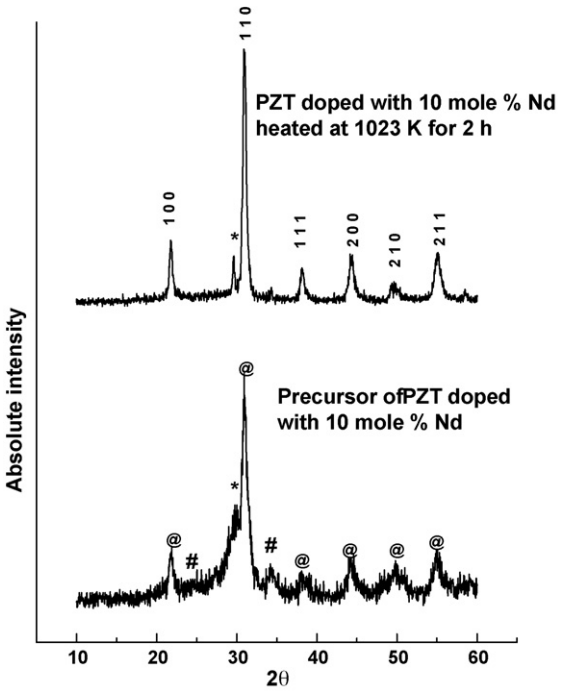


**Fig. 2.** Room temperature XRD patterns of PZT doped with 10 mol% Nd in the precursor stage and calcined stage. (@ = PZT; * = pyrochlore phase; # = impurity phase).

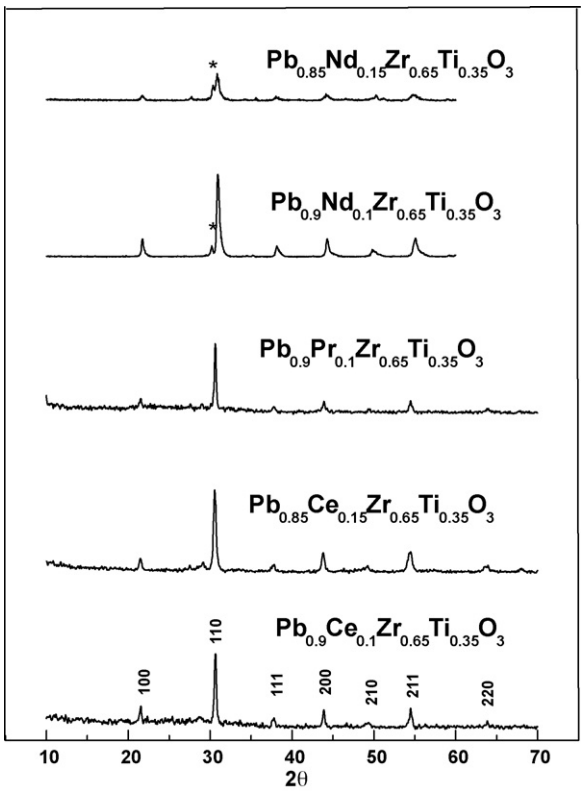


**Fig. 3.** Room temperature XRD patterns of PZT's doped with Nd, Ce and Pr calcined at 1073 K.

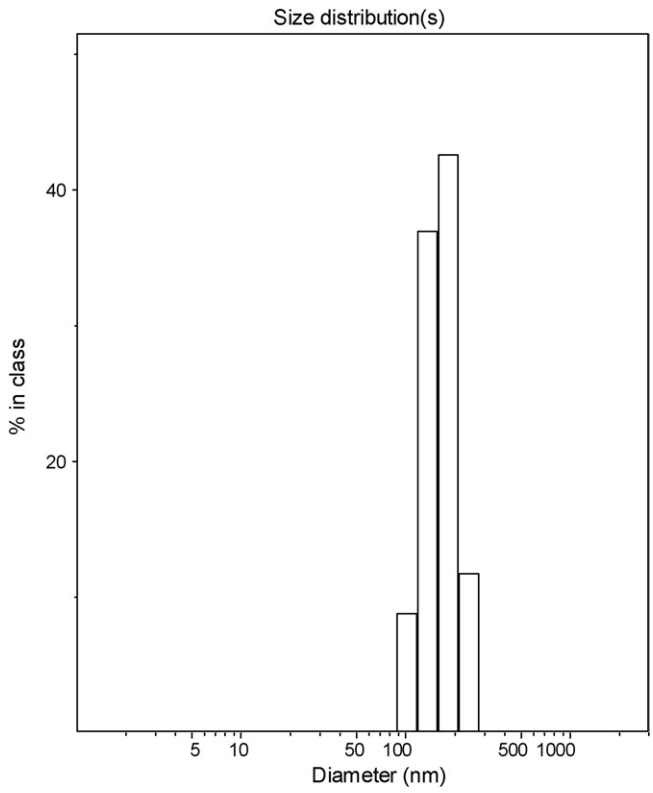


**Fig. 4.** Particle size distribution of PZT doped with 10 mol% of Pr by DLS.

the charge was less than 773 K. The particle size distribution studied by Dynamic Light Scattering (DLS) is shown in Fig. 4 which shows an average particle size of ~280 nm. Fig. 5(a)–(d) shows the SEM photograph of the PZT pellets containing rare earths sintered to 1173 K for 2 h. The microstructure shows spherical, uniform grains of submicron size. The density of the sintered pellet was found to be 94% of Theoretical Density (T.D.). More grain growth was observed in Pr and Ce containing PZT pellets which can be seen from Fig. 5. The density determined by water displacement method showed maximum density for Ce containing samples (varied from 91% to 94% of T.D.) among the series and minimum density for Nd containing samples. The density of Pr doped samples and Nd doped samples determined by water displacement method varied from

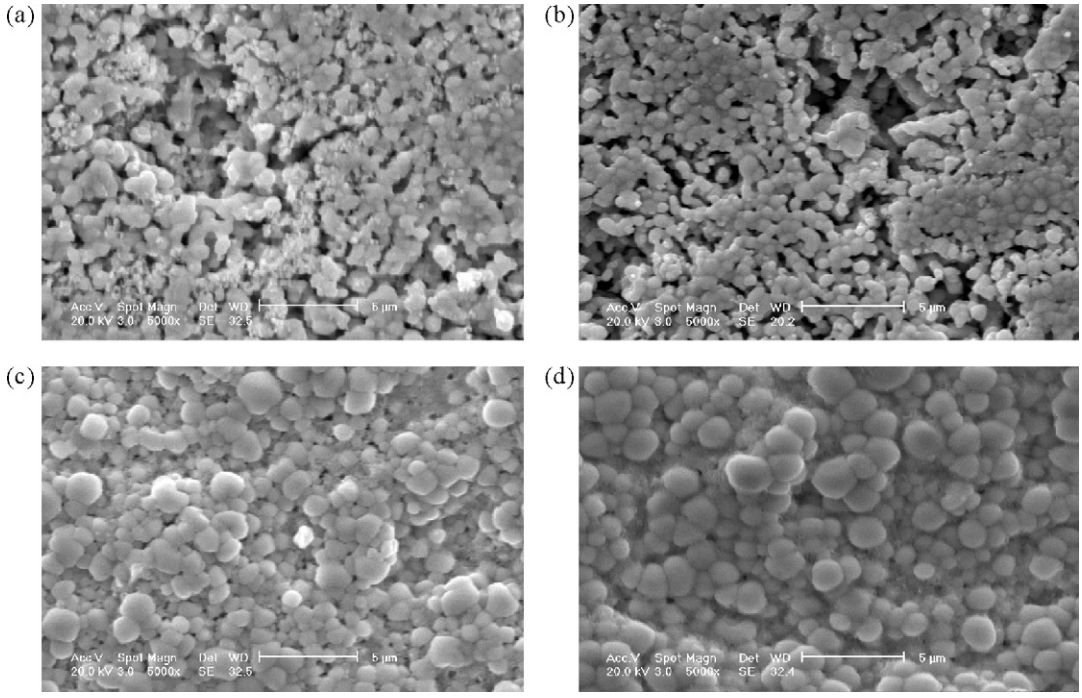


**Fig. 5.** SEM photographs of (a) PZT; (b) PZT containing 10 mol% Nd; (c) PZT containing 10 mol% Pr; (d) PZT containing 10 mol% Ce.

89% to 93% of T.D. and 88–90% of T.D. respectively. Even though the prominent oxidation state for the lanthanides is +3, Ce and Pr can exist in the +4 oxidation as well. Any presence of higher valency is known to incorporate cationic vacancies in the matrix, which is responsible for the enhanced cation diffusivity. The higher densification of Ce and Pr doped samples may be due to this existence of their multi-valent states. The lower value density observed in Nd samples may be due to the presence of pyrochlore phase in these samples.

In integrating the oxide-ferroelectric capacitors into a standard LSI device fabrication process, an annealing step at 350–550 °C in a $H_2$-containing reducing atmosphere is essential. So in order to monitor the redox behaviour and evaluate the compositional stability of these oxides, these samples were subjected to TPR/TPO studies. Fig. 6 shows the TPR profiles of Ce containing PZT (PCeZT), Pr containing PZT (PPrZT) and the base material PZT. Each TPR cycles was followed by TPO cycle. Such four TPR cycles are presented in Fig. 6. The graph shows two different reducing species for the

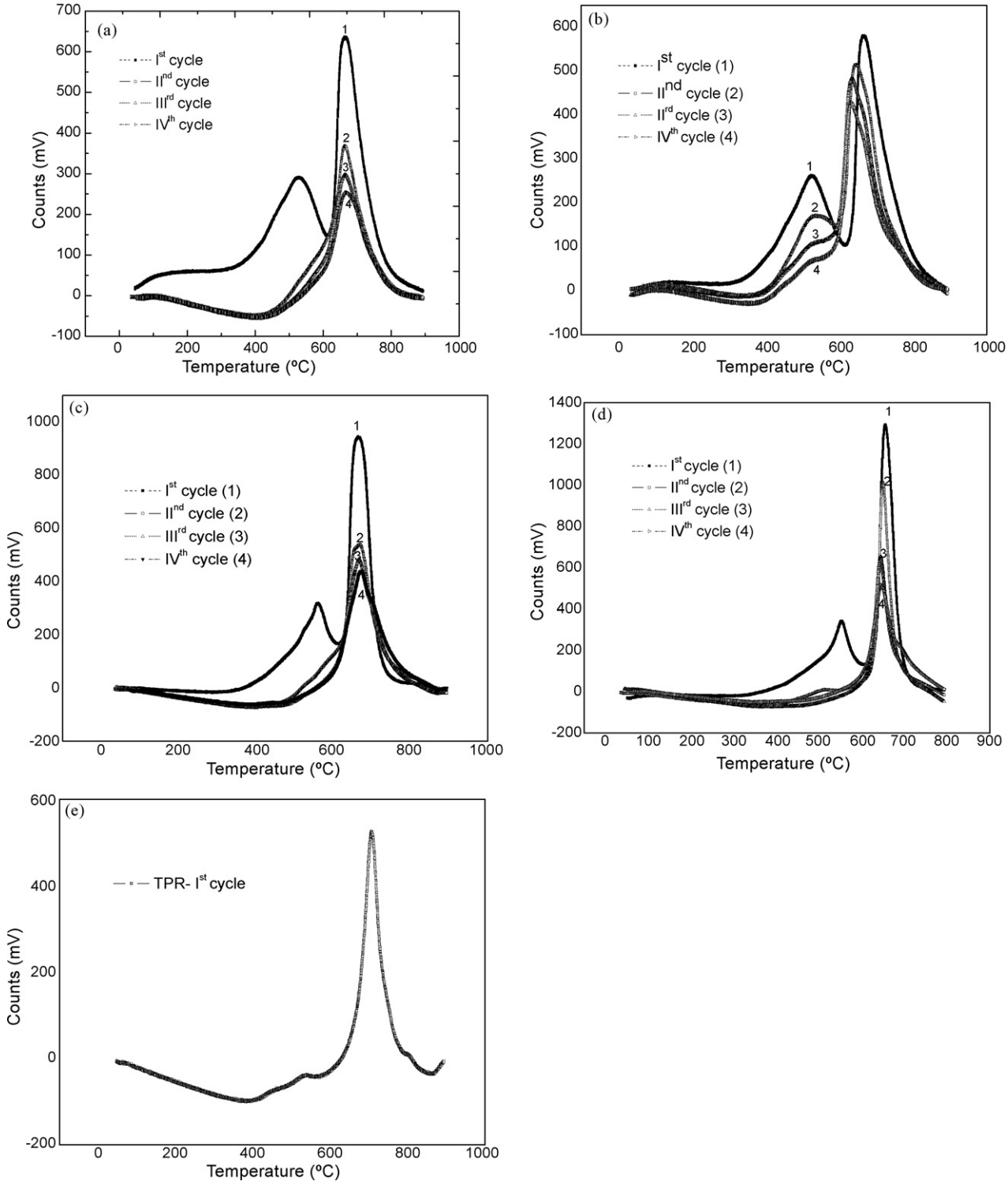


**Fig. 6.** Temperature Programmed Reduction (TPR) profiles of: (a) PCeZT (10 mol%); (b) PCeZT (15 mol%); (c) PPrZT (10 mol%); (d) PPrZT (15 mol%); (e) PZT.

compositions PCeZT and PPrZT where as the undoped PZT sample showed only one reduction step. Even though the prominent oxidation state for the lanthanides is +3, Ce and Pr can exist in the +4 oxidation as well. The first reduction occurred in the case of both PCeZT and PPrZT is attributed to the reduction of this higher oxidation state to +3 oxidation state at around 530 °C. The reduction of lanthanides from higher oxidation state to lower oxidation state could be prominently seen in the first TPR cycle. The subsequent TPR cycles did not clearly show reduction peaks for PPrZT samples whereas the PCeZT samples show reduction peaks due to reduction of $Ce^{4+}$ to $Ce^{3+}$. This can be clearly seen for the sample containing 15 mol% of Ce (b in Fig. 5). This shows that in the case of Ce containing samples even after multiple reductions steps Ce can occupy $Ce^{4+}$ in the perovskite lattice. The 2nd reduction peak appears at around 660 °C in the case of PPrZT and PCeZT and at around 705 °C for undoped sample (PZT) was attributed to the reduction of $Pb^{2+}$ to Pb metal. This shows that the stability of PZT in reducing atmosphere is deteriorating with dopant incorporation in the lattice. Also the stability with respect to temperature of reduction was observed to decrease as we move on from first to fourth TPR cycle which shows the reduction of Pb in the compound to Pb metal at lower temperatures as we move from Ist to IVth TPR cycle. The XRD patterns of residues of TPO (after 3rd TPO cycle) and TPR cycles (after 4th TPR cycle) were recorded and compared with the parent compound. Fig. 7 shows the XRD pattern of TPR/TPO residues of PCeZT samples which were compared with the XRD pattern of initial PCeZT sample. The TPR residues formed showed the presence of Pb metal which formed due to the reduction of $Pb^{2+}$ as well as lanthanide oxide and solid solution of $ZrO_2$ and $TiO_2$. The XRD pattern of TPO residue of PCeZT showed could be compared with that of original PCeZT sample. The XRD pattern of TPO residue of PZT sample (after 4th cycle) could not be compared to the initial PZT. The TPR cycles seemed to degrade the material to such an extent that the oxidation could not restore the original phase. In this sample the major phase was PbO and $ZrO_2$ containing $TiO_2$. Where as in the case of PCeZT, Ce present in the lattice stabilized the original phase and helped in the restoration of the phase whose TPO sample after 4 TPR cycles could be compared with the initial phase.

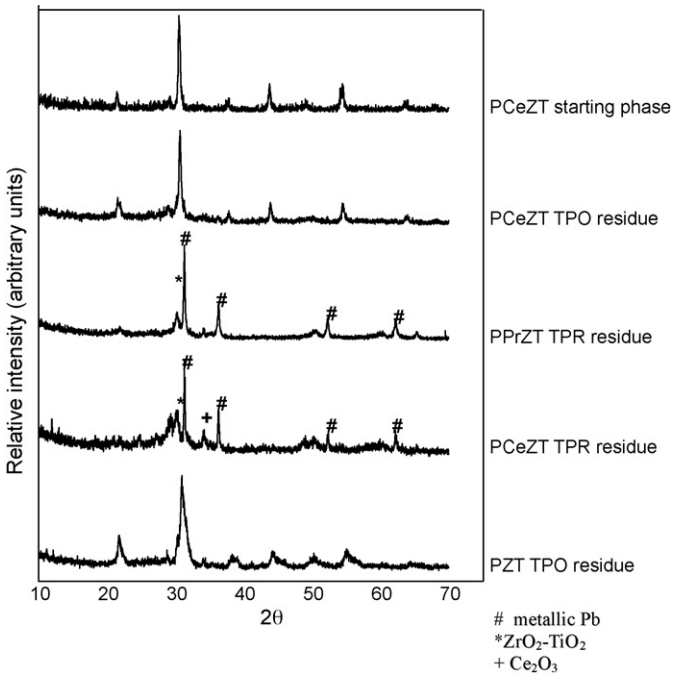


**Fig. 7.** XRD patterns of TPO–TPR residues compared with original compound.

### 3.1. Electrical property measurements by impedance spectroscopy

For impedance measurements, the sintered pellets were polished and coated with a thin layer of Ti paste and heated to 1073 K for 2 h to improve contact with the electrode. The electrical properties of the samples were measured using a Solartron AC Frequency Analyzer (Model 1260) in the frequency range 10 MHz to 1 Hz. Fig. 8 gives the Nyquist plot of the compound $Pb_{0.95}Ce_{0.05}Zr_{0.65}Ti_{0.35}O_3$ at various temperatures. The relaxation frequency ($f_o$) of the material, independently of the geometrical parameter of the sample, was found at the apex of the Nyquist semicircle fulfilling the condition $2\pi f_o R_b C_b = 1$

From this relation, the bulk capacitance of the material ($C_b$), also called the geometric capacitance, can be calculated and the bulk dielectric constant $\varepsilon_b$ can be determined using $C_b = \varepsilon_b \varepsilon_o A/l$; where $\varepsilon_o$ is the vacuum permittivity.

The semicircular pattern in the impedance spectrum is representative of the electrical processes taking place in the material which can be expressed as an equivalent electrical circuit comprising of a parallel combination of resistive and capacitive elements. The intercept of the semicircle on the real axis gives the resistance of the corresponding component contributing towards the impedance of the sample. The graph shows that at lower temperature the resistance offered for conduction is very high. As temperature increases, the conduction becomes easier. This shows typical semiconductor behaviour in these samples. At lower temperature only conduction through grains prevails where as at higher temperature grain conduction as well as grain boundary conduction is seen. The Nyquist plot for PZT undoped and doped with 5 mol% of Pr, Ce and Nd is presented in Fig. 9. The impedance of the sample decreased with Pr doping where as the impedance showed increase with doping of Ce and Nd. The large increase of impedance value in the case of Nd containing samples may be due to the pyrochlore phase present in them.

The frequency (1 Hz to 10 MHz) dependent dielectric constants ($\varepsilon_r$) of all the compounds were determined from the capacitance values. Fig. 10 shows the variation of $\varepsilon_r$ of $PbZr_{0.65}Ti_{0.35}O_3$ as well as $Pb_{0.9}R_{0.1}Zr_{0.65}Ti_{0.35}O_3$ where R = Ce, Pr and Nd as a function of temperature measured at 1 kHz as well as 10 kHz. It is clear that the $\varepsilon_r$ of all the compounds decrease with increase in frequency as the capacitance value of these compounds decreases with increase in frequency. The dielectric constant of these samples increased with increase in temperature as the polarizability of the oxide sys-

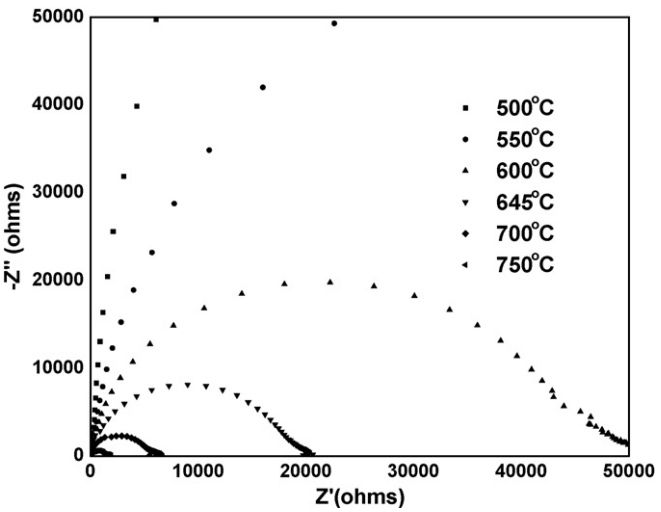


**Fig. 8.** Nyquist plot of $Pb_{0.95}Ce_{0.05}Zr_{0.65}Ti_{0.35}O_3$ at various temperatures.

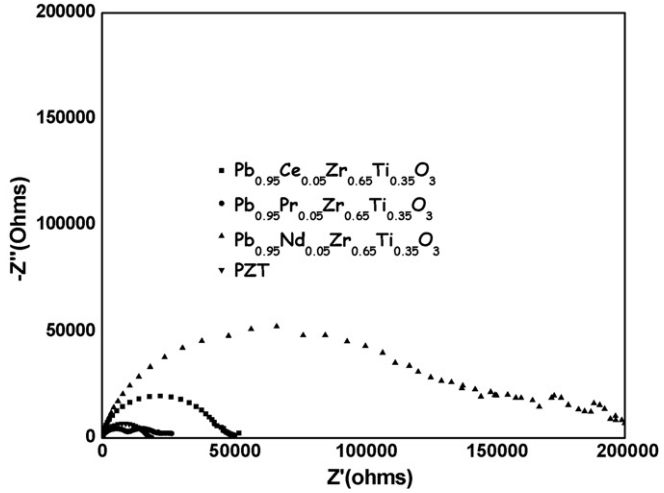


**Fig. 9.** Nyquist plot of PZT containing 5 mol% of rare earths at 600 °C.

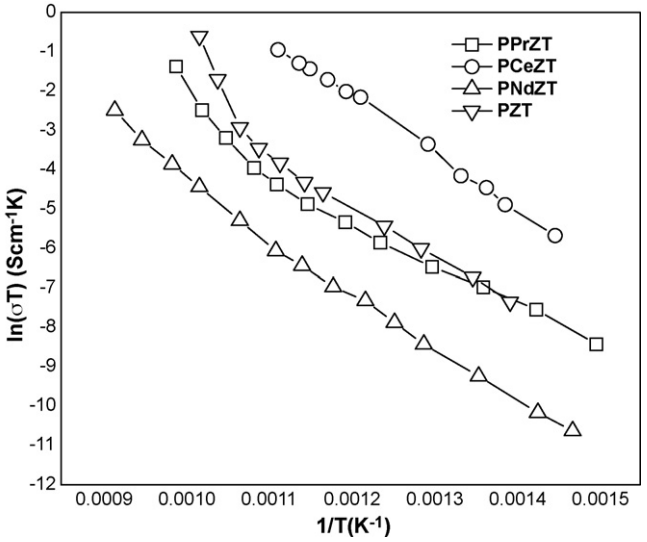


**Fig. 11.** Variation of DC conductivity for PZT and $Pb_{0.85}R_{0.15}Zr_{0.65}Ti_{0.35}O_3$ where R = Ce, Pr and Nd with $1/T$.

tem increases with temperature. Also, it can be seen from the figure that the $\varepsilon_r$ increases with Pr doping in the parent PZT sample where as the $\varepsilon_r$ value remarkably decreases with Ce as well as Nd doping. The sample $Pb_{0.9}Pr_{0.1}Zr_{0.65}Ti_{0.35}O_3$ showed $\varepsilon_r$ of ~22,489 at 710 °C measured at 1 kHz. The undoped samples (PZT) showed a $\varepsilon_r$ of ~19,600 at this temperature whereas Ce and Nd containing samples showed $\varepsilon_r$ values of 5232 and 3002 respectively. Further the dielectric constants of Ce and Nd doped samples were found to decrease with increase in dopant concentration. Shao et al. [23] also reported that the dielectric constant of PZT thin films decreased when the film was doped with Ce. The authors attributed this behaviour to the presence of pyrochlore phase in Ce containing thin films. But in the present study pyrochlore phase was not observed in the Ce containing samples even for 15 mol% of Ce. Ce has almost equal probability to either replace $Pb^{2+}$ at *A* site or $Zr^{4+}/Ti^{4+}$ ions at *B* sites of $ABO_3$ perovskite lattice. This is feasible, as Ce can exist both in tri- and tetra-valence states and can replace $Pb^{2+}$ ($rCe^{3+}$ = 1.43 Å and $rPb^{2+}$ = 1.63 Å) or $Zr^{4+}$ ($rCe^{4+}$ = 0.86 Å and $rZr^{4+}$ = 0.73 Å), respectively. It is reported in the literature [24] that tendency of Ce to occupy A site (as $Ce^{3+}$) is more if the Ce ion concentration is less than 1 mol% and beyond 1 mol%, both *A* as well as *B* site can be occupied by Ce equally ($Ce^{3+}$ in *A* site and $Ce^{4+}$ in *B* site). They further reported that the samples containing Ce in the *A* sites (3+ oxidation state) improve the electrical properties. Similarly, in the present study 5–15 mol% of Ce containing samples may be occupying a large proportion of *B* sites in the $ABO_3$ system which might be responsible for the decreased $\varepsilon_r$ value in the Ce containing PZT. Even though Pr also exhibits tri- and tetra-oxidation states, tri-oxidation state is more stable than tetra-oxidation states whereas in the case of Ce ion, extra stability would be attained by $Ce^{4+}$ ion because of noble gas electronic configuration by removal of 4 electrons. Hence Pr occupancy in *B* sites in place of $Zr^{4+}/Ti^{4+}$is small and high value of $\varepsilon_r$ was observed in the present study. *A* site substitution reduces oxygen vacancies by forming *A* site vacancy–oxygen vacancy defect dipoles causing an increase in electric displacements which subsequently results in increase in the dielectric constant. The donor dopants have been reported to improve the dielectric and ferroelectric properties of PZT thin films [25,26]. Considering the ionic radius of $Nd^{3+}$ (1.0 Å) the *B* site occupancy by Nd should be the minimum. But in our study the addition of Nd in PZT reduces the dielectric constant. This may be due to the presence of pyrochlore phase in the Nd containing samples. During sintering, pyrochlore phase is usually formed as a transient phase before the PZT formation. The pyrochlore phase is oxygen deficient and so it is a metastable transient phase [22]. Thus, in the non-crystallite PZT's, the presence of impurity phases such as pyrochlore play an important role in deciding the dielectric constant.

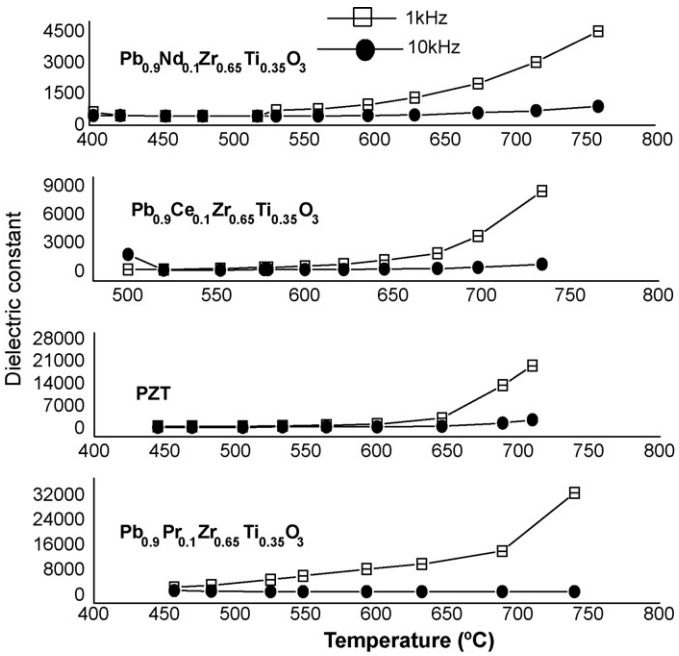


**Fig. 10.** Variation of $\varepsilon_r$ of $PbZr_{0.65}Ti_{0.35}O_3$ as well as $Pb_{0.9}R_{0.1}Zr_{0.65}Ti_{0.35}O_3$ where R = Ce, Pr and Nd as a function of temperature measured at 1 kHz as well as 10 kHz.

The DC conductivity of the samples was calculated using the relation, $\sigma = 1/R^*(l/A)$, where $R$ is the electrical resistance, $l$ the thickness of the sample and $A$ the area of cross section of the sample. The activation energy, $E_a$, for all the samples were calculated from the plot of $\ln(\sigma T)$ versus $1/T$ using the conductivity relation $\sigma T = \sigma_0 \exp(-E_a/(K_B T))$, where $\sigma_0$, is the pre-exponential factor, $E_a$ the activation energy and $K_B$ the Boltzmann constant. The DC conductivity increases with the increase in temperature. At higher temperature, PZT as well as rare earth doped PZT samples behaves as a semiconductor and in semiconducting ceramics, free carriers interact with the charged grain boundaries giving rise to increase in the ionic conductivity. During the course of motion through the solid, the available limited number of mobile carriers gets trapped in relatively stable potential wells. Due to a rise in temperature,

the donor cations take a major part in the conduction process and the conductivity increases. At 10 mol% and 15 mol% dopant concentration, PCeZT showed maximum conductivity among the same class of samples. It was also observed that in PCeZT samples the conductivity increases with increase in dopant concentration whereas for both the Pr and Nd containing samples the conductivity decreases as we increase the dopant concentration. This may be due to the fact that at higher Ce ion concentration, more cationic vacancies are created at *A* site which contributes more towards the conductivity values. The variation of DC conductivity for PZT and $Pb_{0.85}R_{0.15}Zr_{0.65}Ti_{0.35}O_3$ where R = Ce, Pr and Nd with $1/T$ is given in Fig. 11. The conductivity in Nd doped samples showed a minimum value among all the samples and decreased with dopant ion concentration. The amount of pyrochlore phase in the Nd containing samples increased with increase in Nd concentration leading to reduction in the conductivity of these samples.

## 4. Conclusions

Homogeneous, single-phase PZT containing 5, 10 and 15 mol% of Ce and Pr were prepared by a novel solution based technique. But Nd containing samples showed the presence of pyrochlore phases in the calcined powders. The redox behaviour studies concluded that these compounds are stable up to 650 °C. Also these studies showed that dopant incorporation reduces the temperature required for degradation. Ce dopant found responsible for the restoration of initial phases of these compounds when subjected to multiple TPO–TPR cycles. The dielectric constants of PZT decreased with Ce doping because of the B site occupancy whereas the polarizability of samples increases with Pr doping. The DC conductivity of the samples increases with increase in Ce concentration, which may be due to the creation of cationic vacancy at *A* site. The pyrochlore phase in Nd doped samples was found to be responsible for lower conductivity as well as lower dielectric constant values.

## Acknowledgements

The authors wish to express their sincere thanks to Dr. S.K. Aggarwal, Head, Fuel Chemistry Division, for his constant encouragement. We also express our gratitude to Shri Sunil Kumar PIED for his support in carrying out the SEM analysis.

## References

[1] J.N. Kim, M.J. Haun, S. Jm, L.E. Cross, X.R. Xue., IEEE Trans. Ultrason. Ferroelectr. Freq. Control 36 (1989) 4–20.
[2] M.E. Lines, A.M. Glass, Principles and Applications of Ferroelectrics and Related Materials, Oxford, 1979.
[3] S.B. Majumdar, D.C. Agarwal, Y.N. Mohapatra, V.N. Kulkarni, Ferroelectrics 9 (1995) 271–284.
[4] G.A.C.M. Spierings, M.J.E. Ulenaers, G.L.M. Kampschöer, H.A.M. van Hal, P.K. Larsen, J. Appl. Phys. 70 (1991) 2290–2298.
[5] B. Jaffe, W.R. Cook, H. Jaffe, Piezoelectric Ceramics, Academic Press, San Diego, CA, 1971, Chapters 5 and 7.
[6] W.L. Warren, D. Dimos, G.E. Pike, B.A. Tuttle, M.V. Raymond, R. Ramesh, J.T. Evans, Appl. Phys. Lett. 67 (1995) 866–872.
[7] D. Dimos, Annu. Rev. Mater. Sci. 25 (1995) 273–275.
[8] P. Gonnard, M. Troccas, J. Solid State Chem. 23 (1978) 321–326.
[9] M. Troccazs, P. Gonnard, L. Eyraud, Ferroelectrics 22 (1978) 871–874.
[10] H.B. Park, C.Y. Park, Y.S. Hong, K. Kim, S.J. Kim, J. Am. Ceram. Soc. 82 (1999) 94–102.
[11] V.M. Goldschmidt, Skr. Nor. Vidensk.-Akad., 1: Mat. Naturvidensk. Kl. 2 (1926) 8–17.
[12] S.G. Majumder, Y.N. Mohapatra, D.C. Agrawal, J. Mater. Sci. 32 (1997) 2141–2150.
[13] M.J. Akhtar, Z. Akhtar, R.A. Jackson, C.R.A. Catlow, J. Am. Ceram. Soc. 78 (1995) 421–428.
[14] H.D. Sharma, A. Govindan, T.C. Goel, P.K.C. Pillai, C. Pramila, J. Mater. Sci. Lett. 15 (1996) 1424–1426.
[15] P.A. Langjahr, F.F. Lange, T. Wagner, M. Ruhle, Acta Mater. 46 (1998) 773–785.
[16] R.D. Shannon, Acta Crystallogr. A 32 (1976) 751–767.
[17] Y. Tsur, A. Hitomi, A.I. Scrymgeour, C.A. Randall, Jpn. J. Appl. Phys., Part I 40 (2001) 255–258.
[18] S.S. Chnadratreya, R.M. Fulrath, J.A. Pask, J. Am. Ceram. Soc. 64 (1981) 422–425.
[19] B.V. Hiremath, A.I. Kingon, J.V. Biggers, J. Am. Ceram. Soc. 66 (1983) 790–793.
[20] R.V. Kamat, K.T. Pillai, V.N. Vaidya, D.D. Sood, Mater. Chem. Phys. 46 (1996) 67–71.
[21] V. Rajesh, T.V. Pai, Vittal Rao, S.K. Ashok Kumar, V. Mukerjee, Venugopal, J. Alloys Compd 443 (2007) 166–170.
[22] K.G. Brooks, I.M. Reaney, R. Klissurska, Y. Haung, L. Bursill, N. Setter, J. Mater. Res. 9 (1994) 2540–2553.
[23] Q.-Y. Shao, A.-D. Li, Y.-F. Tang, H.-Q. Ling, N.-B. Ming, Mater. Chem. Phys. 75 (2002) 207–210.
[24] S.B. Majumder, D.C. Agrawal, Y.N. Mohapatra, R.S. Katiyar, Mater. Sci. Eng. B 98 (2003) 25–32.
[25] S.H. Lee, S.J. Lee, S.H. Kim, B.G. Chae, Y.S. Yang, H.J. Joo, J.P. Kim, W.S. Park, M.S. Jang, J. Korean Phys. Soc. 32 (1998) 1670–1675.
[26] D.F. Ryder, N.K. Raman, J. Electron. Mater. 21 (1992) 971–975.